Abdominal Radiology (2020) 45:2249–2256
https://doi.org/10.1007/s00261-020-02428-3

SPECIAL SECTION: DISTINGUISHED PAPERS FROM JSAR

A case of focal confluent hepatic fibrosis in the patient with hepatitis C virus-related liver cirrhosis: a mimic of cholangiolocellular carcinoma

Kumi Ozaki[1] · Masaki Takeshita[2] · Katsuhiko Saito[3] · Hirohiko Kimura[1] · Toshifumi Gabata[4]

Published online: 5 February 2020

Abstract

During routine ultrasound examination, a hyperechoic mass was detected in the anterior segment of the liver in an 80-year-old woman with hepatitis C virus-related cirrhosis. Computed tomography and magnetic resonance imaging findings suggested a malignant tumor with abundant fibrous stroma, similar to cholangiolocellular carcinoma. However, subsequent partial hepatectomy revealed a mass characterized by abundant fibrosis without tumor cells, dilated blood vessels, and marginal ductular reaction. Accordingly, focal confluent fibrosis was diagnosed. Generally, the diagnosis of focal confluent fibrosis is straightforward because of its well-established imaging characteristics. However, its differentiation from a malignant tumor can occasionally be difficult because of variation in presentation depending on the amount of fibrous stroma and the degree of inflammatory cell infiltration. In the present case, diagnosis was difficult because the lesion was more localized than usual, presenting a mass-like shape, and there was obvious hyperintensity on T2-weighted imaging and ring-shaped hyperintensity on diffusion-weighted imaging. Moreover, hepatic capsular retraction was indistinct, which can be one of the key findings of focal confluent fibrosis. When a hepatic mass is associated with a fibrous lesion, focal confluent fibrosis should be considered in the differential diagnosis, even though the lesion is associated with several atypical findings.

Keywords Confluent hepatic fibrosis · Cholangiolocellular carcinoma · Cholangiocellular carcinoma · Cirrhosis · Ductular reaction

Introduction

Focal confluent fibrosis is commonly encountered in patients with end-stage cirrhosis, particularly in those with alcoholic cirrhosis [1–3], although it has also been described in patients with early-stage cirrhosis and cirrhosis with any etiology. Imaging findings of focal confluent fibrosis have been reported [1–4], and these established imaging characteristics facilitate its diagnosis. However, this condition can present with various findings and enhancement patterns, and it sometimes mimics the findings of malignant tumors such as intrahepatic cholangiocarcinoma including cholangiolocellular carcinoma, hepatocellular carcinoma, and metastases [1, 2, 4–7].

Here we report the case of surgically resected focal confluent fibrosis that mimicked cholangiolocellular carcinoma on preoperative computed tomography (CT) and magnetic resonance (MR) imaging.

Case report

An 80-year-old woman was referred to our hospital for further examination of a new hepatic mass detected during routine ultrasound examination. The patient was previously diagnosed with hepatitis C virus-related cirrhosis and diabetes mellitus, but she had not undergone periodic surveillance of the hepatic lesions for the last 6 years. She had no history of alcohol abuse.

Laboratory analysis indicated that the patient was in a hyperglycemic state [blood sugar, 224 mg/dL (normal

✉ Kumi Ozaki
ozakik-rad@umin.org

1 Department of Radiology, Faculty of Medical Sciences, University of Fukui, 23-3 Matsuoka-Shimoaizuki, Eiheiji, Fukui 910-1193, Japan

2 Department of Surgery, Toyama City Hospital, Toyama, Japan

3 Diagnostic Pathology, Toyama City Hospital, Toyama, Japan

4 Department of Radiology, Kanazawa University Graduate School of Medicine, Kanazawa, Japan

range, 70–110 mg/dL); HbA1c, 11.6% (normal range, 4.6%–6.2%)]. Other biochemical test results were within the normal range. However, alpha-fetoprotein levels were slightly elevated [28.0 ng/dL (normal range, < 10 ng/dL)], whereas other tumor marker levels were within the normal range including those of prothrombin induced by vitamin K absence-II [15 mAU/mL (normal level, < 40 mAU/mL)], carcinoembryonic antigen [4.3 ng/mL (normal range, < 5 ng/mL)], and carbohydrate antigen 19–9 [31.7 U/mL (normal range, < 37 U/mL)]. The indocyanine green plasma disappearance rate was delayed [24% (normal level, < 15%)].

Ultrasound imaging of the liver showed an ill-defined hyperechoic mass in the anterior segment (Fig. 1). Contrast-enhanced CT imaging was performed using a CT system. Following unenhanced CT, a contrast material with 600 mg iodine per kilogram of body weight was injected with an injection duration of 30 s. The arterial dominant phase was determined using the bolus-tracking method and obtained 35 s after the injection. The portal dominant phase (65 s after the injection) and equilibrium phase (150 s after the injection) were obtained. On noncontrast CT, the liver showed a nodular contour compatible with cirrhotic morphology. An ill-defined, low-density mass (27 mm at its largest diameter) was visible in the anterior segment (Fig. 2a); this was absent in a prior CT examination performed 6 years ago. Dynamic contrast-enhanced CT images showed that the mass had an irregular margin and that it was hypovascular, with gradual enhancement from the periphery (Fig. 2b–d). Dimpling of hepatic surface was also observed (Fig. 2e), and intratumoral vessels were observed within the mass (Fig. 2f, g). The anterior segment had decreased in volume compared with that observed in a prior CT examination performed 6 years ago (Fig. 3a, b).

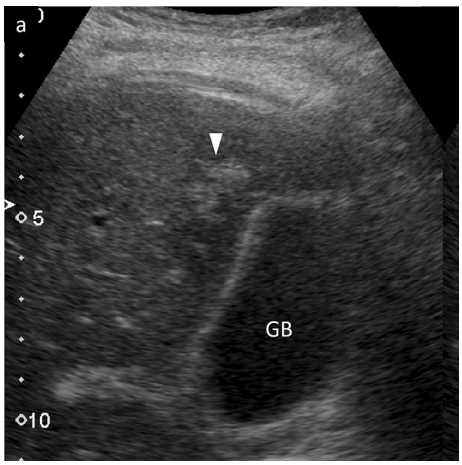

Fig. 1 Ultrasound image. Ultrasonography revealed an ill-defined hyperechoic lesion in the anterior segment of the liver (arrowhead). *GB* gall bladder

MR images were obtained using a 1.5 T MR system. On MR imaging, no focal fat deposits were observed within the mass on in-phase [repetition time (TR)/echo time (TE)/flip angle (FA) = 6.7/4.8 ms/10°] and opposed-phase (TR/TE/FA = 6.7/2.4 ms/10°) images (Fig. 4a, b), and the mass showed obvious hyperintensity on T2-weighted (TR/TE/FA = 1000/86 ms/150°) and fat-suppressed T2-weighted (TR/TE/FA = 3300/70 ms/160°) images (Fig. 4c, d). The mass exhibited a ring-shaped hyperintensity on diffusion-weighted image (TR/TE/FA = 2500/55 ms/90°; *b*-value, 800) (Fig. 3e). There was no decrease in the apparent diffusion coefficient (ADC) values (2.15×10^{-3} mm^2/s), and the ring shape was obscure (Fig. 4f). Dynamic contrast study was performed with a transverse plane using a fat-suppressed three-dimensional T1-weighted spoiled gradient-echo sequence (TR/TE/FA = 3.4/1.3 ms/12°). After obtaining precontrast images, the patient received a dose of 0.1 mL/kg Gd-EOB-DTPA (Primovist; Bayer Schering Pharma, Berlin, Germany) intravenously at a rate of 1.0 mL/s, followed by a 20-mL saline flush. Immediately after the start of the Gd-EOB-DTPA injection, dynamic studies were performed using the test injection method (1.5 mL of Primovist + 8-mL saline flush), and arterial phase timing was determined as the peak time of the abdominal aorta plus 10 s half of imaging time. Portal dominant and transient phase images were obtained at 70 and 150 s after the injection. Transverse and coronal hepatobiliary phase images were obtained at 20 min after the injection. Dynamic contrast-enhanced MR images showed that the mass had an irregular margin and that it was hypovascular, with gradual enhancement from the periphery (Fig. 5a–d); furthermore, it showed hypointensity on hepatobiliary phase image (Fig. 5e). The configuration of the lesion presented a mass-like form on axial CT and MR images (Figs. 2, 4, and 5), but a wedge-shaped appearance toward hepatic surface was presented on the coronal hepatobiliary phase image (Fig. 5f).

Several other hypovascular nodules were observed, all approximately 5 mm in diameter; each nodule showed different findings on CT and MR imaging (Fig. 6). These nodules were also absent in the prior CT examination performed 6 years ago. No fluorine-18 fludeoxyglucose (FDG) uptake was observed in any lesion on positron emission tomography–CT (Fig. 7).

Regarding the largest lesion in segment 5, CT and MR findings suggested a malignant tumor with abundant fibrous stroma, particularly cholangiolocellular carcinoma, classified in the latest World Health Organization classification as a small duct-type intrahepatic cholangiocarcinoma [8]. Although the enhancement pattern was not typical of cholangiolocellular carcinoma, which is often characterized by intratumoral vessels, the arterial enhancement, ring-shaped hyperintensity on diffusion-weighted images, and lack of FDG uptake were almost consistent with a tumor

Fig. 2 Computed tomography (CT) images. On noncontrast CT, the liver showed a nodular contour compatible with cirrhotic morphology. An ill-defined low-density mass was observed in the anterior segment (arrowhead) (**a**). On dynamic contrast-enhanced CT images, the mass presented as a hypovascular lesion with gradual enhancement from the periphery (**b**–**d**; **b** arterial phase; **c** portal phase; **d** equilibrium phase). The dimpling of hepatic surface was observed (arrowhead) (**e**) [CT slice located 2.5 cm caudal to the upper CT images (**a**–**d**)]. Intratumoral vessels were observed within the mass (**f**–**h**; maximum-intensity projection images with a slab thickness of 3 mm) (arrowheads)

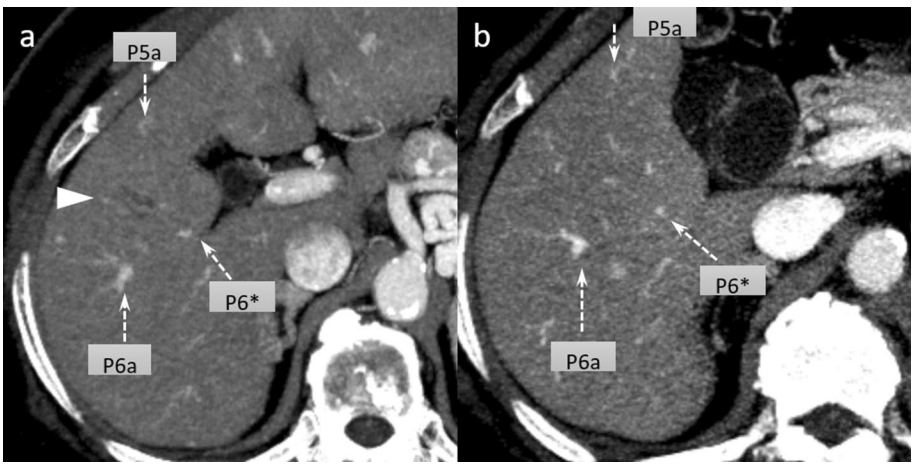

Fig. 3 CT images. The region mainly including segment 5 enclosed by portal branches (arrows) (**a**) decreased compared with that observed in a prior CT examination 6 years ago (**b**). The hypovascular lesion present in the center of the region (arrowhead) (**a**). CT images were maximum-intensity projection images with a slab thickness of 3 mm

accompanied by abundant fibrosis such as cholangiolocellular carcinoma. Meanwhile, other small hypovascular nodules were considered to be low- or high-grade dysplastic nodules that appear during multistep hepatocarcinogenesis considering the patient's background of hepatitis C virus-related liver cirrhosis.

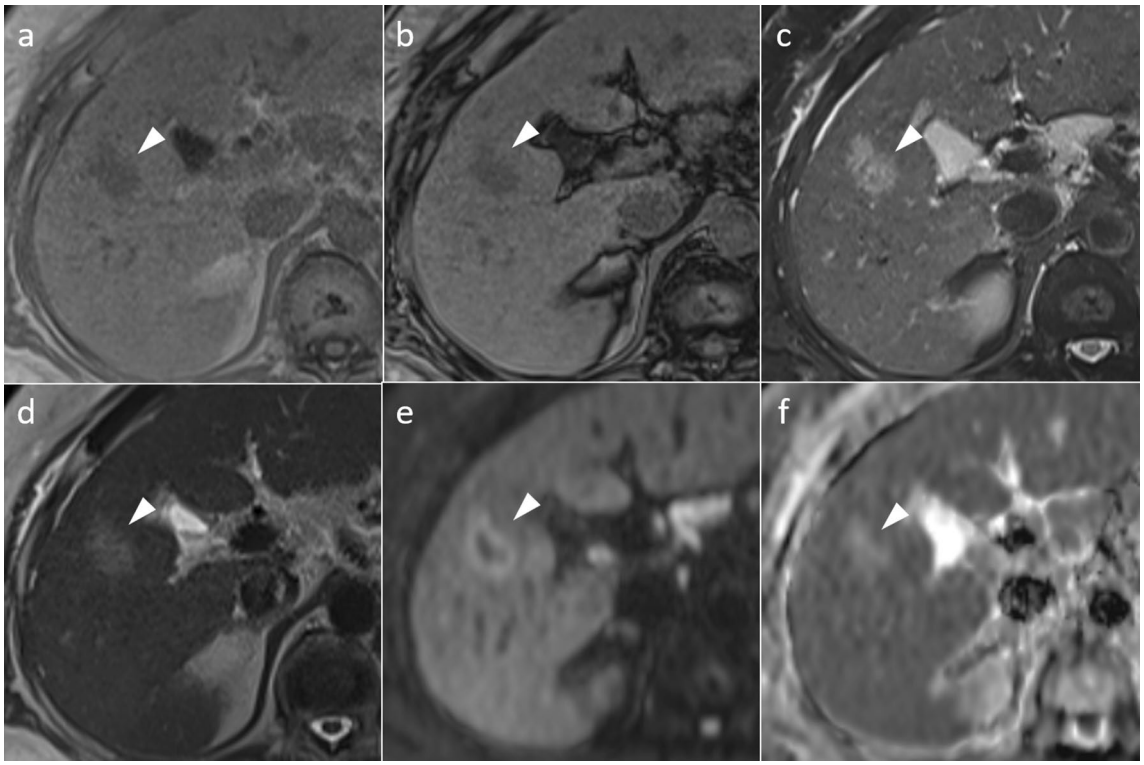

Fig. 4 Magnetic resonance images. No focal fat deposits were observed within the mass on in-phase (**a**) and opposed-phase (**b**) images (arrowheads). The mass was ill-defined and showed obvious hyperintensity on fat-suppressed T2-weighted (**c**) and T2-weighted (**d**) images. The mass exhibited ring-shaped hyperintensity on the diffusion-weighted image (**e**), but there was no decrease in the apparent diffusion coefficient values (**f**)

After obtaining full informed consent, laparoscopic hepatic subsegmental resection of only fibrous lesion on segment 5 was performed because of the patient's insufficient hepatic functional reserve, as shown by the indocyanine green plasma disappearance rate (24%). The small hypovascular nodules were subjected to periodic monitoring.

The resected specimen was an ill-defined, white mass approximately 3 cm in diameter that contained dilated blood vessels (Fig. 8a). Histopathologically, hematoxylin and eosin and azan staining showed that the mass primarily comprised abundant fibrosis and dilated blood vessels. However, no tumor cells were detected. Background parenchyma comprised regenerative nodules of varying sizes and fibrosis classified as METAVIR stage F4, consistent with the diagnosis of cirrhosis (Fig. 8b–d). In addition, ductular reaction and inflammatory cell infiltration were observed to be spreading into the borderline between the mass and background parenchyma (Fig. 8e). Based on these findings, the mass was diagnosed as focal confluent fibrosis related to cirrhosis.

Discussion

Repeated liver injury due to acute and chronic inflammation from various causes results in the excessive deposition of collagen, proteoglycans, and other macromolecules in the extracellular matrix, known as fibrosis, on a rare occasion. Progressive hepatic fibrosis ultimately leads to cirrhosis, in which fibrous bands divide the liver parenchyma into regenerative nodules [9]. This is a characteristic feature of almost all types of end-stage liver disease.

This fibrous change commonly spreads diffusely throughout the entire liver. However, there can infrequently be strong fibrosis in a localized area of unknown cause, referred to as focal confluent fibrosis [1, 2]. This presents as broad fibrotic scars, with imaging findings including a focal, often wedge-like shape from the region of the porta hepatis to the liver capsule, with associated capsular retraction and volume loss, most often involving the anterior and medial segments [1–4].

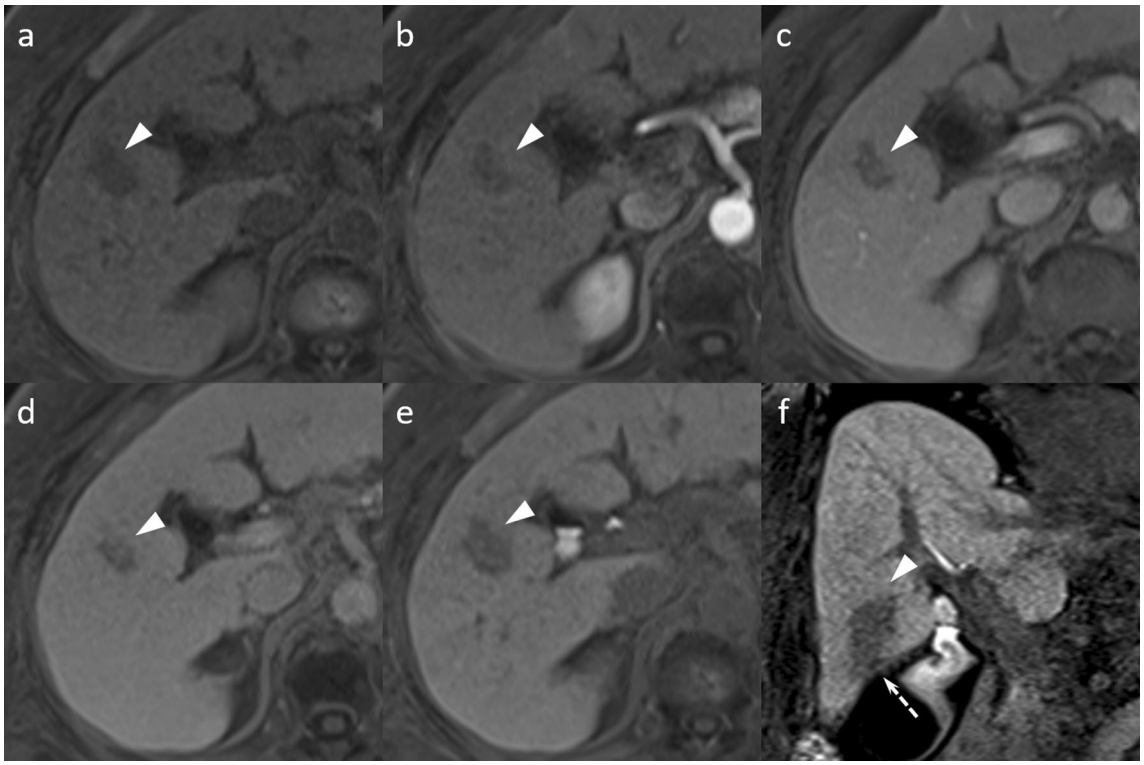

Fig. 5 Dynamic contrast (gadoxetic acid)-enhanced magnetic resonance image**.** The mass presented hypointensity on precontrast T1-weighted imaging with fat suppression (**a**) and appeared hypovascular with gradual enhancement from the periphery (arrowheads) (**a**–**d**). (**a**, precontrast; **b**, arterial phase; **c**, portal phase; **d**, transitional phase) The mass showed hypointensity on the hepatobiliary phase image (arrowheads) (**e**, **f**)

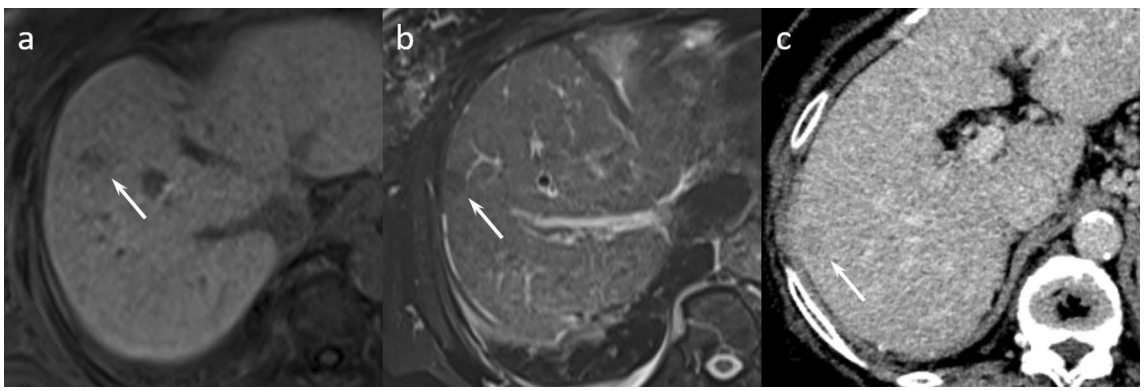

Fig. 6 Imaging of other nodules. **a**–**c** Several other small nodules, approximately 5 mm in diameter, were observed (arrows) (**a** hepatobiliary phase; **b** fat-suppressed T2-weighted image; **c** equilibrium phase CT). The nodules were hypovascular, and each nodule presented different findings

Hepatic capsular retraction (defined as a focal irregularity, flattening, or concavity of the normally convex border of the liver capsule) is associated with several types of hepatic lesions, both benign and malignant [10]. It is one of the key findings of focal confluent fibrosis, although the dimpling in the present lesion could not be referred to as capsular retraction.

These characteristic morphological changes generally present as hypoattenuation on noncontrast CT images, hypointensity on T1-weighted images, and moderate hyperintensity on T2-weighted images. On dynamic contrast-enhanced CT and MR imaging, the enhancement is principally gradual and delayed [1, 2], although various enhancement patterns can be observed [5, 11–14]

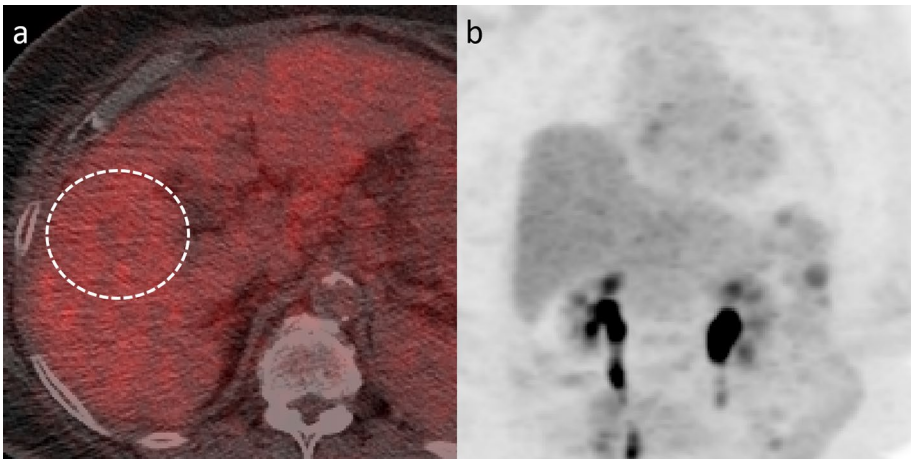

Fig. 7 Positron emission tomography-computed tomography (PET–CT). No uptake of fluorine-18 fludeoxyglucose was detected in the mass on PET–CT (**a**) or maximum-intensity projection (**b**) images

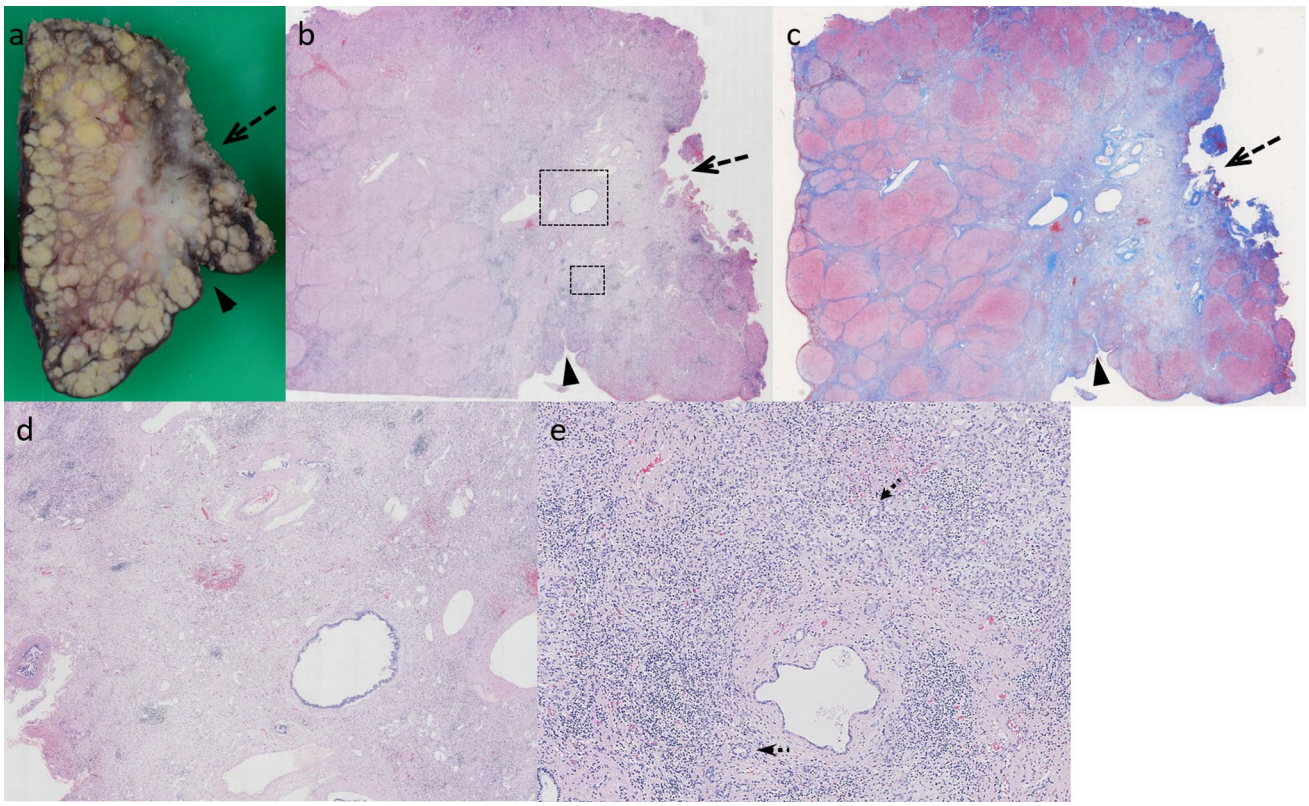

Fig. 8 Macroscopic and microscopic findings of the resected specimen. **a** The resection specimen showed an ill-defined, white mass containing dilated blood vessels. Concavity of the hepatic surface could be seen (arrowhead). The arrow indicates the end of hepatectomy. **b–d** Background parenchyma included small regenerative nodules. Microscopically, the mass comprised abundant fibrosis and dilated blood vessels, with no tumor cells detected. Azan staining clearly showed abundant fibrosis within the mass (**c**). Background parenchyma comprised regenerative nodules of varying sizes and fibrosis classified as METAVIR stage F4 (**b**, **c**). [**b** hematoxylin and eosin (HE) staining, original magnification, ×10; **c** azan staining, ×20; **d** HE staining, ×20]. **e** Ductular reactions (arrows) and inflammatory cell infiltration were observed to be spreading into the borderline between the mass and background parenchyma (HE, original magnification, ×40)

including arterial phase hyperenhancement that mimics malignancies such as hepatocellular carcinoma and intrahepatic cholangiocarcinoma [15–17]. The variety of enhancement patterns depends on contrast retention that varies according to the amount of fibrous stroma present in the lesion and the degree of inflammatory cell infiltration, which vary depending on the different periods of fibrous change [18, 19], and the degree of neovascularization or

arterial flow input also varies. The gradual enhancement observed in the present case was typical of focal confluent fibrosis but the mass-like shape could indicate a fibrous tumor.

The mean ADC of the confluent fibrosis is significantly greater than that of background cirrhotic liver parenchyma [20], although the reported ADC values showed wide variability in both benign and malignant lesions. In addition, marginal hyperintensity on diffusion-weighted images has not been reported. We speculated that the marginal hyperintensity observed on the diffusion-weighted image in the present case could be corresponding with the pathological findings of ductular reaction and inflammatory cell infiltration, although it was just a speculation. Moreover, the discrepancy between T2- and diffusion-weighted images and the ADC map has not been elucidated.

In general, it is not difficult to diagnose focal confluent fibrosis because of its well-established characteristic imaging findings and location [1–4]. However, several other findings in the present case made it difficult to distinguish the lesion from a neoplasm accompanied by abundant fibrosis. First, the lesion was more localized than usual, presenting a mass-like shape, and the characteristic wedge-like shape radiating from the porta hepatis was obscure. Second, capsular retraction was also ambiguous because of the relative localization of the lesion. Third, the ring-shaped hyperintensity observed on diffusion-weighted images resembled an intrahepatic cholangiocarcinoma with abundant fibrosis [21, 22], although its ADC value was higher than that of background cirrhotic liver parenchyma. Fourth, the lack of FDG uptake generally indicates that a lesion is benign, but it has recently been reported that such a finding is also consistent with the diagnosis of cholangiolocellular carcinoma [23]. Lastly, penetrating vessels within the mass can be observed in intrahepatic cholangiocarcinoma including cholangiolocellular carcinoma [24, 25], although the dilatation of the intrahepatic bile ducts in the periphery of the mass is commonly observed in intrahepatic cholangiocarcinoma [26, 27]. In addition, hepatitis C virus-related cirrhosis is a risk factor for intrahepatic cholangiocarcinoma progression [28, 29].

In conclusion, the present case illustrated the difficulty experienced in distinguishing focal confluent fibrosis from cholangiolocellular carcinoma on a rare occasion. When a hepatic mass is associated with a fibrous lesion, focal confluent fibrosis should be considered in the differential diagnosis to avoid excessive treatment.

Funding This study received no specific grant from any funding agency.

Compliance with ethical standards

Conflict of interest The authors declare that they have no conflicts of interest.

Ethical approval All procedures performed in studies involving human participants were in accordance with the ethical standards of the institutional and/or national research committee and with the 1964 Helsinki Declaration and its later amendments or comparable ethical standards.

Informed consent The requirement for written informed consent was waived for this case report on the basis of the opt-out system of our institution.

References

1. Ohtomo K, Baron RL, Dodd GD 3rd et al (1993) Confluent hepatic fibrosis in advanced cirrhosis: appearance at CT. Radiology 188(1):31–35. https://doi.org/10.1148/radiology.188.1.8511316
2. Ohtomo K, Baron RL, Dodd GD 3rd et al (1993) Confluent hepatic fibrosis in advanced cirrhosis: evaluation with MR imaging. Radiology 189(3):871–874. https://doi.org/10.1148/radiology.189.3.8234718
3. Ozaki K, Matsui O, Gabata T, Kobayashi S, Koda W, Minami T (2013) Confluent hepatic fibrosis in liver cirrhosis: possible relation with middle hepatic venous drainage. Jpn J Radiol 31(8):530–537. https://doi.org/10.1007/s11604-013-0222-8
4. Brancatelli G, Baron RL, Federle MP, Sparacia G, Pealer K (2009) Focal confluent fibrosis in cirrhotic liver: natural history studied with serial CT. AJR Am J Roentgenol 192(5):1341–1347. https://doi.org/10.2214/AJR.07.2782
5. Kelekis NL, Makri E, Vassiou A, Patsiaoura K, Spiridakis M, Dalekos GN (2004) Confluent hepatic fibrosis as the presenting imaging sign in nonadvanced alcoholic cirrhosis. Clin Imaging 28(2):124–127. https://doi.org/10.1016/S0899-7071(03)00243-2
6. Kim SK, Kim SR, Imoto S et al (2016) Confluent hepatic fibrosis in alcohol liver cirrhosis with elevated pivkaii value - usefulness of immunostaining for EZH2 and p16(INK4a) in differentiating it from cholangiolocellular carcinoma - Confluent hepatic fibrosis. Pathol Int 66(9):543–545. https://doi.org/10.1111/pin.12435
7. Park YS, Lee CH, Kim BH et al (2013) Using Gd-EOB-DTPA-enhanced 3-T MRI for the differentiation of infiltrative hepatocellular carcinoma and focal confluent fibrosis in liver cirrhosis. Magn Reson Imaging 31(7):1137–1142. https://doi.org/10.1016/j.mri.2013.01.011
8. Paradis V, Fukayama M, Park YN, Schirmacher P (2019) Tumors of the liver and intrahepatic bile ducts. In: WHO classification of tumours of the digestive system, 5th edn. IARC, Lyon, pp 215-264
9. Wallace K, Burt AD, Wright MC (2008) Liver fibrosis. Biochem Genet 411(1):1–18. https://doi.org/10.1042/BJ20071570
10. Blachar A, Federle MP, Sosna J (2009) Liver lesions with hepatic capsular retraction. Semin Ultrasound CT MR 30(5):426–435
11. Husarik DB, Gupta RT, Ringe KI, Boll DT, Merkle EM (2011) Contrast enhanced liver MRI in patients with primary sclerosing cholangitis: inverse appearance of focal confluent fibrosis on delayed phase MR images with hepatocyte specific versus extracellular gadolinium based contrast agents. Acad Radiol 8(12):1549–1554. https://doi.org/10.1016/j.acra.2011.08.007
12. Ooi CG, Chan KL, Peh WC, Saing H, Ngan H (1999) Confluent hepatic fibrosis in monozygotic twins. Pediatr Radiol 29(1):53–55. https://doi.org/10.1007/s002470050534

13. Ahn IO, de Lange EE (1998) Early hyperenhancement of confluent hepatic fibrosis on dynamic MR imaging. AJR Am J Roentgenol 171(3):901–902. https://doi.org/10.2214/ajr.171.3.9725360
14. Matsuo M, Kanematsu M, Kondo H et al (2001) Confluent hepatic fibrosis in cirrhosis: ferumoxides-enhanced MR imaging findings. Abdom Imaging 26(2):146–148. https://doi.org/10.1007/s002610000181
15. Galia M, Taibbi A, Marin D et al (2014) Focal lesions in cirrhotic liver: what else beyond hepatocellular carcinoma? Diagn Interv Radiol 20(3):222–228. https://doi.org/10.5152/dir.2014.13184
16. Itai Y, Saida Y (2002) Pitfalls in liver imaging. Eur Radiol 12(5):1162–1174. https://doi.org/10.1007/s00330-001-1178-0
17. Brancatelli G, Federle MP, Ambrosini R et al (2007) Cirrhosis: CT and MR imaging evaluation. Eur J Radiol 61(1):57–69. https://doi.org/10.1016/j.ejrad.2006.11.003
18. Semelka RC, Chung JJ, Hussain SM et al (2001) Chronic hepatitis: correlation of early patchy and late linear enhancement patterns on gadolinium-enhanced MR images with histopathology initial experience. J Magn Reson Imaging 13(3):385–391. https://doi.org/10.1002/jmri.1055
19. Martin DR, Lauenstein T, Kalb B et al (2012) Liver MRI and histological correlates in chronic liver disease on multiphase gadolinium-enhanced 3D gradient echo imaging. J Magn Reson Imaging 36(2):422–429. https://doi.org/10.1002/jmri.23668
20. Mwangi I, Hanna RF, Kased N et al (2010) Apparent diffusion coefficient of fibrosis and regenerative nodules in the cirrhotic liver at MRI. AJR Am J Roentgenol 194(6):1515–1522. https://doi.org/10.2214/AJR.09.3484
21. Maetani Y, Itoh K, Watanabe C et al (2001) MR imaging of intrahepatic cholangiocarcinoma with pathologic correlation. AJR Am J Roentgenol 176(6):1499–1507. https://doi.org/10.2214/ajr.176.6.1761499
22. Park HJ, Kim YK, Park MJ, Lee WJ (2013) Small intrahepatic mass-forming cholangiocarcinoma: target sign on diffusion-weighted imaging for differentiation from hepatocellular carcinoma. Abdom Imaging 38:793–801. https://doi.org/10.1007/s00261-012-9943-x
23. Takahashi Y, Sato S, Ishitobi H et al (2017) Intrahepatic Cholangiolocellular and Cholangiocellular Carcinoma - Differences in the 18F-FDG PET/CT Findings. Intern Med 56(22):3027–3031. https://doi.org/10.2169/internalmedicine.8839-17
24. Kaneko K, Honda H, Kajiyama K et al (1996) Radiologically identifiable intratumoral portal vein in intrahepatic cholangiomas: a diagnostic pitfall. Abdom Imaging 21(5):445–447. https://doi.org/10.1007/s002619900100
25. Haradome H, Unno T, Morisaka H et al (2017) Gadoxetic acid disodium-enhanced MR imaging of cholangiolocellular carcinoma of the liver: imaging characteristics and histopathological correlations. Eur Radiol 27(11):4461–4471. https://doi.org/10.1007/s00330-017-4811-2
26. Zhao YJ, Chen WX, Wu DS, Zhang WY, Zheng LR (2016) Differentiation of mass-forming intrahepatic cholangiocarcinoma from poorly differentiated hepatocellular carcinoma: based on the multivariate analysis of contrast-enhanced computed tomography findings. Abdom Radiol (NY) 41(5):978–989. https://doi.org/10.1007/s00261-015-0629-z
27. Yoshimitsu K, Honda H, Kaneko K et al (1997) MR signal intensity changes in hepatic parenchyma with ductal dilation caused by intrahepatic cholangiocarcinoma. J Magn Reson Imaging 7(1):136–141. https://doi.org/10.1002/jmri.1880070119
28. Donato F, Galatti U, Tagger A et al (2001) Intrahepatic cholangiocarcinoma and hepatitis C and B virus infection, alcohol intake, and hepatolithiasis: a case-control study in Italy. Cancer Causes Control 12(10):959–964. https://doi.org/10.1023/a:1013747228572
29. Perumal V, Wang J, Thuluvath P, Choti M, Torbenson M (2006) Hepatitis C and hepatitis B nucleic acids are present in intrahepatic cholangiocarcinomas from the United States. Hum Pathol 37(9):1211–1216. https://doi.org/10.1016/j.humpath.2006.04.012